A precision tool for dissecting orbital dynamics in time-dependent potentials

Courtlandt L. Bohn and Balša Terzić
Department of Physics, Northern Illinois University, DeKalb, IL 60115

We develop a technique for dissecting orbital dynamics in time-dependent potentials. A given orbit may be regular, exhibiting periodicity; chaotic, exhibiting a continuum of frequencies; or intermittent, exhibiting transitions between these two behaviors. We show how to construct a function from the orbital dynamics alone that reveals the behavior of the orbit, including transient chaos, if present. It also pinpoints the transition times for intermittent orbits within an uncertainty of just a few characteristic orbital periods. This fast indicator appears to be generic and independent of the dimensionality of the system.

PACS numbers: 05.45.-a, 45.10.-b, 41.75.-i, 98.10.+z

The ability to characterize orbital dynamics in time-dependent potentials, e.g., nonequilibrium systems, is the key to understanding such systems. If this can be done 'instantaneously', then one has in effect a phase-space microscope with which to monitor the onset and evolution of instabilities, most notably ones that are triggered on a local scale. To wit, by integrating all of the initial conditions comprising the system and dissecting the behavior of each respective orbit, one can color-code each orbit at every time step, the color signifying whether it is regular or chaotic at that time, and thereby make high-resolution movies of the evolving phase space of the system. A fast, precise measure of orbital dynamics is thereby a holy grail in the context of nonequilbrium systems.

A common measure of chaos is the Lyapunov exponent [1]. This measure is a time-averaged quantity where the time average is over an infinite interval; hence, it is restricted exclusively to *time-independent* systems. In fact, most of the techniques for characterizing orbits involve the convergence of a measure, whereby the convergence requires a long integration time [2]. This circumstance has motivated alternative methods, most notably frequency analysis [3], that circumvent the need for convergence, but these schemes still require at least tens of orbital periods to yield a reliable characterization. Moreover, all methods devised to date have serious difficulty dealing with sticky orbits (those that are regular for an extended time and then become chaotic) and intermittent orbits (those that transition randomly between regular and chaotic behavior; such transitions may occur quickly and frequently [4]). One promising method for circumventing all of these problems involves time-series analysis based on pattern recognition of signals associated with Poincaré sections of orbital epochs [5]. This method, still under development, is applicable to both time-independent and time-dependent potentials. However, it requires orbital integration sufficiently long to form the pattern, typically ∼10 orbital periods.

An obvious tactic is to compute the 'tangent dynamics', i.e., the 'tangent separation' $|Z| = (Z_i Z^i)^{1/2}$ between two hypothetical, initially neighboring orbits in the potential V:

$$\ddot{Z}^i + (\partial^i \partial_j V) Z^j = 0; \;\; Z(0) = \epsilon, \; \dot{Z}(0) = 0, \qquad (1)$$

where ϵ is small. For regular (chaotic) orbits, Z should exhibit a power-law (exponential) dependence on time t. The logarithm of $Z(t)$ is a measure of the '*instantaneous* Lyapunov exponent' at time t (differing from the conventional Lyapunov exponent defined in the limit $t \to \infty$).

In this paper we present a method for efficiently dissecting orbital behavior in time-dependent potentials. It is based on dynamics alone, and (as we demonstrate) it yields much higher resolution than can be obtained from $Z(t)$. Our method devolves from computing an integral of motion I following the method of Struckmeier and Riedel (SR) [6]. We show that an auxiliary function $f(t)$ that is solved as part of computing I provides precise information needed to characterize the orbit. Our analysis involves a Vlasov-Poisson picture; we follow the orbits of test particles in a smooth potential. These particles move according to the potential but add nothing to it.

By carefully following the procedure in SR, we obtain for the integral of particle motion in a smooth time-dependent potential $V(\mathbf{x}, t)$:

$$I = f(t)H - (1/2)[\dot{f}(t)\mathbf{x}\cdot\mathbf{p} - (1/2)\ddot{f}(t)|\mathbf{x}|^2 - c(t)], \qquad (2)$$

in which H is the Hamiltonian and $f(t)$ is the solution of the 3^{rd}-order differential equation

$$\begin{aligned} &(1/2)|\mathbf{x}|^2 f^{(3)} + (2V + \mathbf{x}\cdot\nabla V)\dot{f} + 2(\partial_t V)f + \dot{c} = 0; \\ &f(0) = 1, \;\; \ddot{f}(0) = \dot{f}(0) = 0, \;\; c(0) = 0. \end{aligned} \qquad (3)$$

The idea is to solve for the orbit $(\mathbf{x}, \mathbf{p})$ while simultaneously solving for the auxiliary function $f(t)$. The initial conditions are such that $I = H(\mathbf{x}, \mathbf{p}, t = 0)$ for all time. The second auxiliary function $c(t)$ is absent in SR and in their follow-on work [7]. It represents a gauge freedom, i.e., $c(t)$ can be chosen for convenience in solving Eq. (3).

In applying their formalism to several charged-particle-beam examples, SR note that $f(t)$ will often exponentially diverge during the evolution of an orbit [7]. They comment that "physical implications that are associated with an unstable behavior of $f(t)$... remain to be investigated", and that "this instability is not necessarily associated with an instability of the beam moments". They leave open the question as to what is happening, save to remark that this circumstance "may indicate a transition from a regular to a chaotic motion". This juncture marks our starting point.

We shall consider orbits in two example potentials. The first is a one-dimensional (1D) charged-particle-beam potential (a breathing spherical 'waterbag'). The analytics of this model are cumbersome, but its physical features are simple. What is most interesting is that, when breathing, it supports a population of chaotic orbits that all originate within the waterbag's density profile. It also supports a population of orbits that intermittently change from regular to chaotic and vice versa, as well as a population of orbits that get injected to large amplitudes and form a beam halo. In short, though the model is physically simple, it supports dynamically intricate orbits, making it an excellent choice for developing and testing diagnostics of chaos. The second example involves a 3D galactic potential (a harmonically perturbed 'Dehnen-like' potential). It likewise supports a rich array of orbital dynamics.

The spherical waterbag is comprised of radial orbits. It mimicks a spherical beam bunch under the influence of a linear focusing force and an internal repulsive space-charge force [8]. Its equilibrium potential derives from a distribution function $g(r,p) = \mathcal{N}[H_0 - H(r,p)]^{-1/2}$ for $H < H_0$; g is zero otherwise, and H_0 is a constant. The density $\rho(r)$ for a bunch of total charge Q (found by integrating $g(r,p)$ over momentum space) and the potential $V(r)$ (found by solving Poisson's equation) are:

$$\rho = [3Q/(4\pi R^3\nu)]\{1 - i_0[r/(R\alpha)]/i_0(\xi)\}, \tag{4}$$

$$\begin{aligned} V = &\left\{[\nu/(\xi R\alpha)] - (1/2)(1-R^{-3})[(\xi R\alpha)^2 \right. \\ &\left. -r^2] - (\mu/R)d_0[r/(R\alpha)]\right\}\Theta(\xi R\alpha - r) \\ &-\left\{(1/2)[(\xi R\alpha)^2 - r^2] - (\nu/r)\right\}\Theta(r - \xi R\alpha), \end{aligned} \tag{5}$$

wherein $\Theta(y)$ is the Heaviside step function. Auxiliary quantities in these expressions are:

$$\begin{aligned} &i_0(y) \equiv y^{-1}\sinh y, \quad d_0(y) \equiv i_0(\xi) - i_0(y), \\ &\alpha \equiv \left\{\frac{(3+\xi^2)i_0(\xi) - 3\cosh\xi}{[\xi^4 + 15(2+\xi^2)]i_0(\xi) - 5(6+\xi^2)\cosh\xi}\right\}^{\frac{1}{2}}, \\ &\mu \equiv \frac{3\alpha^2}{i_0(\xi)}, \quad \nu \equiv \frac{\xi\alpha^3}{i_0(\xi)}[(3+\xi^2)i_0(\xi) - 3\cosh\xi], \end{aligned}$$

in which the intermediary parameter ξ is found from the space-charge tune depression η by solving

$$\frac{15}{4i_0(\xi)}\frac{(12+5\xi^2)i_0^2(\xi) - 3[3i_0(\xi)+\cosh\xi]\cosh\xi}{[30+\xi^2(15+\xi^2)]i_0(\xi) - 5(6+\xi^2)\cosh\xi} = \eta^2,$$

and R is the envelope radius.

By populating the sphere with test particles and letting it oscillate homologously, one has a 'particle-core model' [9] with a nonuniform density that establishes a nonlinear space-charge force on the test particles. This is accomplished by letting R be a function of time determined by the dimensionless 'envelope equation'

$$\ddot{R} + R - \frac{\eta^2}{R^3} - \frac{1-\eta^2}{R^2} = 0; \; R(0) = M, \; \dot{R}(0) = 0. \tag{6}$$

The length scale is the equilibrium envelope radius, the time scale is the inverse of the angular external focusing frequency, and M is the 'mismatch'. Thus, the waterbag comprises a two-parameter (η, M) family of models; we take $\eta = 0.15$ and M=0.5. We take each test particle, without loss of generality, to be confined to the x-axis; thus, the equation of motion is $\ddot{x} = -\partial_x V$. The density is generally nonuniform. Nonetheless, orbits in the static sphere (M=1) are integrable due to the spherical symmetry. However, the breathing sphere supports a significant population of chaotic orbits, as is likewise true in a cylindrical waterbag [10].

To solve for $f(t)$ from Eq. (3), one must first choose a gauge $c(t)$ to cancel terms that diverge when the particle passes through the origin, thereby circumventing the respective instability. An obvious choice is:

$$\begin{aligned} &\dot{c} = [(\xi R\alpha)^2 - \zeta/R]\dot{f} + [2(\xi\alpha)^2R^3 + \zeta](\dot{R}/R^2)f; \\ &\zeta \equiv (\xi\alpha)^2 + 2[\nu/(\xi\alpha) - \Delta], \quad \Delta \equiv \mu[i_0(\xi) - 1], \end{aligned}$$

with which Eq. (3) becomes, after dividing by $x^2/2$:

$$\begin{aligned} f^{(3)} + 4\Big\{&\Big[\{1 - R^{-3} - (Rx^2)^{-1}Q[x/(R\alpha)]\}\dot{f} \\ &+R^{-2}\{3/2 + x^{-2}K[x/(R\alpha)]\}\dot{R}f\Big]\,\Theta(\xi R\alpha - |x|) \\ &+\{1 - (2x^2)^{-1}(\zeta/R - \nu/|x|)\dot{f} \\ &+\zeta[2(Rx)^2]^{-1}\dot{R}f\}\Theta(|x| - \xi R\alpha)\Big\} = 0, \end{aligned} \tag{7}$$

wherein the auxiliary functions $K(y)$ and $Q(y)$ are

$$\begin{aligned} K(y) &\equiv \mu[d_0(y) + j_0(y)] - \Delta, \\ Q(y) &\equiv K(y) - \mu j_0(y)/2, \; j_0(y) \equiv i_0(y) - \cosh y. \end{aligned}$$

The procedure is then to solve Eq. (7) as part of a system of differential equations that includes the equation of test-particle motion.

Consider Fig. 1, which pertains to an orbit that originates well within the beam envelope and eventually gets ejected to large amplitudes. We plot there the orbit itself, the auxiliary function $f(t)$ vs. t, and the tangent-separation function $Z(t)$. Note that orbital transitions are much more sharply delimited by $f(t)$ than by $Z(t)$. Most importantly, Fig. 1 shows that using $f(t)$ as a dynamical indicator "works". At early times, the orbit lingers in the deep interior where the waterbag density is nearly uniform, and in turn it is regular ($\log_{10}|f(t)|$ plateaus). The orbit stays regular for a considerable time and hence is 'sticky'. Later it gets 'unstuck' and migrates toward a 2:1 resonance with the breathing oscillation; it becomes chaotic during this migration ($\log_{10}|f(t)|$ grows). Eventually the resonant coupling becomes strong enough to eject the particle to large amplitudes. Now, when the particle lingers far from the breathing waterbag density (the 'core'), it experiences predominantly the linear focusing force. Hence, when moving on large amplitudes, the orbit *must* be regular, and this is exactly what Fig. 1 shows. There is a 'beating' at this stage as

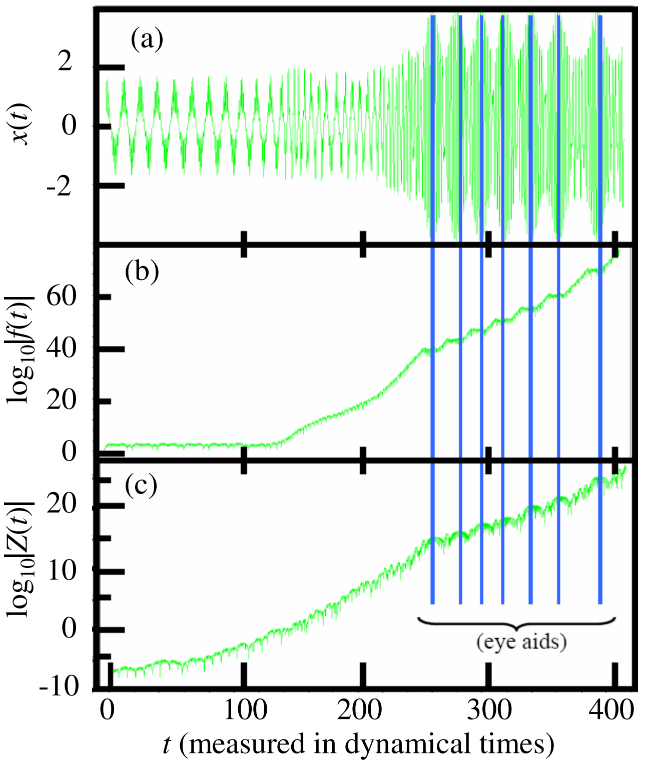

FIG. 1: An example intermittent 'halo orbit' in the waterbag: (a) the trajectory $x(t)$ vs. t; (b) $\log_{10}|f(t)|$ vs. t; (c) $\log_{10}|Z(t)|$ vs. t. Time is measured in dynamical times (periods of the envelope oscillation). The lines aid the eye to emphasize the regularity of large-amplitude orbital segments.

the orbit intermittently falls out of, then back into, resonance. When out of resonance, the orbit spends most of its time close to or in the core, i.e., migrating back toward resonance, and the orbit is thus again chaotic, as is indicated. We have thereby verified this 'indicator of chaos' $f(t)$ against the known physics of the model. One sees that $f(t)$ gives a crisp, correct, and virtually *immediate* indication of transitions between regular behavior and chaotic behavior. By contrast, the tangent separation $Z(t)$ does not.

A second example of a sticky intermittent orbit is the subject of Fig. 2(a,b). As $f(t)$ indicates [Fig. 2(a)], this orbit begins regular, transitions to chaotic, then transitions back to regular (and later, not shown, becomes chaotic again). The intersections of the hand-drawn 'slopes' indicate the transition times. As one can infer, these times are pinpointed to within a few dynamical times, and this 'method' by which we extracted them suggests a way to automate this diagnostic, a subject for a future paper. As evident from the Poincaré plot [Fig. 2(b)], this orbit gets unstuck from a KAM torus, then restuck near the same torus, a behavior consistent with the labeling of the segments inferred from $f(t)$.

We now turn to the harmonically perturbed 3D

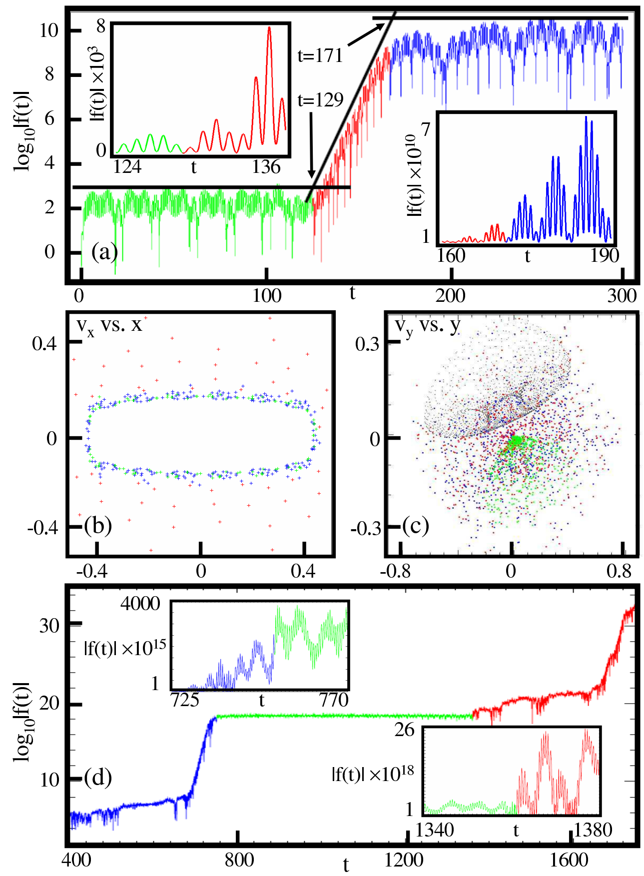

FIG. 2: Example analyses of intermittent orbits in the waterbag (a,b) and Dehnen (c,d) potentials. Concerning waterbag: (a) $\log_{10}|f(t)|$ vs. t and (insets) localized plots of $|f(t)|$ vs. t; (b) corresponding stroboscopic Poincaré surface of section. Colors indicate regular (green, blue) and chaotic (red) epochs, as inferred from the behavior of $f(t)$. In (b) a phase-space point is plotted each time $R(t)$ takes its minimum value, the points corresponding to $t \in$[0,129] (green), $t \in$(129,171] (red), and $t \in$(171,300] (blue). Note that *only* red points are found in the 'chaotic sea' of (b). Concerning Dehnen: (c) Poincaré surface of section; (d) corresponding $|\log_{10} f(t)|$ vs. t and (insets) localized plots of $|f(t)|$ vs. t. Time is measured in crossing times (the time between successive orbital crossings of the (y, z)-plane). Colors now indicate chaotic (blue, red) and regular (green) epochs. In (c) the points correspond to the unperturbed (m=0) potential (black), $t \in$[0,751] (blue), $t \in$(751,1361] (green), and $t \in$(1361,2000] (red). Note that the perturbation immediately jettisons the orbit into a chaotic sea. Later it is relatively confined (green points), but then gets jettisoned again.

Dehnen-like potential $V(\mathbf{x}, t)$:

$$V = -(2-\gamma)^{-1}(1 + m \sin \omega t)\{1 - [s/(1+s)]^{2-\gamma}\}, \quad (8)$$

where $s^2 = (x/a)^2 + (y/b)^2 + (z/c)^2$ with a, b, c denoting ellipsoidal semiaxes, m is the amplitude and ω is the frequency of the harmonic perturbation. This potential originates from the spherical Dehnen potential [11]; it is defined in terms of the ellipsoidal coordinate s instead of the radial coordinate r. The spherical Dehnen potential provides a good fit to inner regions of many elliptical galaxies. We choose $\gamma = 0$ (corresponding to a density profile without a central cusp), m=0.2, ω=2, and $a^2 : b^2 : c^2 = 1.00 : 0.95 : 0.90$. Most, if not all, orbits in the unperturbed (m=0) Dehnen potential are regular. Introducing the harmonic perturbation causes many orbits to become chaotic through resonant phase mixing [12].

Eq. (3) now becomes, upon dividing by $s^2/2$:

$$f^{(3)} + [1 + m\sin\omega t]\{[(3+2s)/(1+s)^3] - 2s^{-2}\}\dot{f} + 2m\omega\cos\omega t[(1+s)^{-2} - s^{-2}]f + \dot{c} = 0. \qquad (9)$$

The 3^{rd}, 4^{th}, and 5^{th} terms cause instabilities: the 3^{rd} near $s = 0$, the 4^{th} near $\cos\omega t = 0$, and the 5^{th} near both $s = 0$ and $\cos\omega t = 0$. If we choose a gauge $\dot{c}(t)$ to cancel these problematic terms, then the solution of Eq. (9) with initial conditions $f(0) = 1$, $\ddot{f}(0) = \dot{f}(0) = 0$, is trivial: $f = 1$ for all t. Thus, instead, we start the orbit integration using $c(t) = 0$ for a few time steps and, before the instability sets in, we then turn on $c(t)$ to cancel the problematic terms.

Fig. 2(c,d) concerns an intermittent orbit in this Dehnen-like potential. As the Poincaré section indicates [Fig. 2(c)], the perturbation immediately ejects the particle out of the phase space it would have occupied had it not been perturbed. The behavior of $f(t)$ [Fig. 2(d)] strongly suggests that the orbit starts off chaotic ($\log_{10}|f(t)|$ grows), during which time it migrates through an appreciable volume of the phase space, then becomes regular ($\log_{10}|f(t)|$ plateaus), being confined near a 2:1 resonance (as we saw by plotting the orbit). Later it becomes chaotic again, sampling a large volume of phase space, and finally it is ejected to infinity.

We remarked initially that $f(t)$ is an auxiliary function associated with computing the integral of motion I per Eq. (2). This integral is analytically exact. However, as $f(t)$ and its derivatives diverge, the computed integral likewise diverges due to roundoff errors from subtracting large, nearly equal numbers. This can be circumvented easily by occasionally renormalizing and restarting the computation. The moral is that use of this formalism depends on the user's interest. Checking the conservation of I along an orbit and checking the dynamical behavior of an orbit require different strategies.

To summarize, we constructed a precision indicator of orbital behavior in time-dependent potentials. The indicator $f(t)$ devolves from constructing the integral of motion I, and thus is based on dynamics alone. We demonstrated its use in conjunction with a 1D and 3D potential; although we discuss only a few orbits here, we studied many, and in every case the indicator worked as described. We also looked at a 2D potential (a harmonically perturbed dihedral potential [13]), and again, the indicator worked as described here. Thus, it appears the indicator is generic, i.e., independent of the dimensionality of the potential. Because one can also construct the integral I in N-body ($3N$-dimensional) systems [7], we expect $f(t)$ likewise to be useful for studying orbital dynamics in simulations of those systems, and this will be a topic of future work. One seeming complication, one that is often but not always inherent to this application, is the need to choose a gauge to cancel terms that cause instabilities in the differential equation for $f(t)$. For the cases we studied, we found that the qualitative behavior of $f(t)$, hence its usefulness as a precision indicator of orbital dynamics, is insensitive to the choice of gauge, provided the gauge satisfactorily cancels the problematic terms.

This work was supported by the Department of Education under Grant No. P116Z010035, and by the Department of Energy under Grant No. DE-FG02-04ER41323.

[1] G.L. Benettin, A. Galgani, and J.M. Strelcyn, Phys. Rev. A **14**, 2338 (1976).
[2] G. Contopoulos G., *Order and Chaos in Dynamical Astronomy* (Springer-Verlag, Berlin, 2002).
[3] J. Laskar, Icarus **88**, 266 (1990).
[4] H.E. Kandrup, I.M. Vass, and I.V. Sideris, Mon. Not. Roy. Astron. Soc. **341**, 927 (2003).
[5] I.V. Sideris, Ann. NY Acad. Sci. **1045**, 79 (2005); Phys. Rev. E (in preparation).
[6] J. Struckmeier and C. Riedel, Phys. Rev. Lett. **85**, 3830 (2000).
[7] J. Struckmeier and C. Riedel, Phys. Rev. E **64**, 026503 (2001).
[8] R.L. Gluckstern and A.V. Fedotov, Phys. Rev. ST Accel. Beams **2**, 054201 (1999).
[9] T.P. Wangler, K.R. Crandall, R. Ryne, and T.S. Wang, Phys. Rev. ST Accel. Beams **1**, 084201 (1998).
[10] H. Okamoto and M. Ikegami, Phys. Rev. E **55**, 4694 (1997).
[11] W. Dehnen, Mon. Not. Roy. Astron. Soc. **265**, 250 (1993).
[12] B. Terzić, H.E. Kandrup, Mon. Not. Roy. Astron. Soc. **347**, 957 (2004).
[13] I.V. Sideris, in Proceedings of the Particle Accelerator Conference, Knoxville, 2005 (in press).